

ELECTRICAL BEHAVIOR OF A  $\text{Cu}_2\text{Fe}_{1-x}\text{Co}_x\text{SnS}_4$  CERAMIC

FERNANDA LÓPEZ-VERGARA, ANTONIO GALDÁMEZ Y VÍCTOR MANRÍQUEZ

Departamento de Química, Facultad de Ciencias, Universidad de Chile, Santiago, Chile  
(Received: September 2, 2013 - Accepted: September 30, 2013)

## ABSTRACT

The solid solutions  $\text{Cu}_2\text{Fe}_{1-x}\text{Co}_x\text{SnS}_4$ , with stannite-type structure are stable up to about 800°C. The electrical properties of the  $\text{Cu}_2\text{Fe}_{0.4}\text{Co}_{0.6}\text{SnS}_4$  ceramic were investigated by complex impedance. The real and imaginary dielectric permittivity dependence with the temperature were measured between 10kHz and 1 MHz in temperature range 77-280K, finding that the ceramic present the characteristics behavior of a dielectric relaxation between 100 and 250 K, with a maximum at approximately 200 K. The electric permittivity found has orders of magnitude between  $10^2$  and  $10^3$ . A space charge polarization mechanism is suggested to explain the observed electric relaxation.

**Key words:** *Quaternary sulfides, dielectric relaxation, stannite*

## INTRODUCTION

Quaternary  $\text{Cu}_2\text{M}^{\text{II}}\text{M}^{\text{IV}}\text{S}_4$  sulfides have been the subject of a variety of research due to their interesting properties, which are technologically useful. Their potential technical applications include uses as nonlinear optics [1,2], photovoltaic absorbers [3–5], and thermoelectric materials at high temperature [6,7].

These sulfides are known as diamond semiconductor materials because they crystallize in the stannite structure derived from the diamond family [8,9]. The technological applications of these materials have made them the subjects of extensive studies to determine their physical properties, including the magnetic properties of these quaternary sulfides, particularly the stannite  $\text{Cu}_2\text{FeSnS}_4$  [10,11].

However, the electrical properties of these quaternary sulfides have been studied by various techniques. Using the Van der Pauw method on single crystals, the conductivities and the activation energies of  $\text{Cu}_2\text{CoGeS}_4$  and  $\text{Cu}_2\text{MnSnS}_4$  were determined, and the obtained conductivity values were 7.69 S/cm and 6.25 S/cm, respectively. The activation energy was found to be 0.03 eV at room temperature [1]. In a subsequent study using this same technique, it was determined that  $\text{Cu}_2\text{CdGeS}_4$  also has an  $E_a = 0.03$  eV [12]. In addition, using theoretical calculations it was estimated that the band gaps ( $E_g$ ) were approximately 1.5 eV in  $\text{Cu}_2\text{ZnSnS}_4$  and 1.0 eV in  $\text{Cu}_2\text{ZnSnSe}_4$  [2,13]. Recently, a number solid solutions derived from  $\text{Cu}_2\text{ZnSnS}_4$  (CZTS), due to their potential applications as absorbent photovoltaic solutions in solar cells have been the object of thin-film electrical characterization using the measurements of the Hall effect and photoluminescence, and they have been shown to reach efficiency up to 10.1% [3–5].

To study the dielectric character of this type of compound, it is necessary to use complex impedance measurements in samples that have been previously transformed into ceramics, which presents a challenge for this type of phase. The electroceramics are usually formed by oxides, and all of the thermal processes are carried out in air conditions. Publications describing electroceramics based on chalcogenides are rare because of the oxidation of these compounds. Previously, our group studied new solid solutions from different families of quaternary sulfide stannites, such as  $\text{Cu}_2\text{Mn}_{1-x}\text{Co}_x\text{SnS}_4$  [14],  $\text{Cu}_2\text{Mn}_x\text{Fe}_{1-x}\text{SnS}_4$  and  $\text{Cu}_2\text{Fe}_{1-x}\text{Co}_x\text{SnS}_4$ , and this last family is focus of the current study.

In this paper, we describe the preparation and characterization of the electroceramics from solid solutions of the type  $\text{Cu}_2\text{Fe}_{1-x}\text{Co}_x\text{SnS}_4$  and its end-members,  $\text{Cu}_2\text{CoSnS}_4$  and  $\text{Cu}_2\text{FeSnS}_4$ ; in particular, the electrical behaviour of a  $\text{Cu}_2\text{Fe}_{0.4}\text{Co}_{0.6}\text{SnS}_4$  ceramic was studied.

## MATERIALS AND METHODS

## 2.1 Synthesis

The polycrystalline  $\text{Cu}_2\text{Fe}_{1-x}\text{Co}_x\text{SnS}_4$  compounds were prepared by direct combination of powders of the corresponding high purity elements (99.99%, Aldrich) in stoichiometric amounts. All manipulations were carried out under Argon atmosphere. The reaction mixture was sealed in evacuated quartz ampoules, placed in a programmable furnace, heated to 850 °C for about 72

hours, and then cooled by quenching in liquid nitrogen. The products appeared to be air- and moisture-stable over several weeks.

## 2.2 Powder X-ray diffraction measurements

Powder X-ray diffraction patterns were collected, at room temperature, on Siemens D5000 powder diffractometer, with  $\text{CuK}_\alpha$  radiation ( $\lambda = 1.541871$  Å) in the range  $5^\circ < 2\theta < 80^\circ$ . The XRD patterns were indexed with the computer program CHECKCELL [15].

## 2.3 SEM-EDS analysis

The chemical compositions of the samples were determined by scanning electron microscopy with the aid of energy-dispersive X-ray analysis (SEM-EDS) using a JEOL 5400 system equipped with an Oxford LinK ISIS microanalyzer. The working distance was 35 mm and the accelerating voltage was set to 22.5 kV. Samples were mounted onto double-sided carbon tape, which was adhered to an aluminum specimen holder. EDS data were collected for 60 s. A FE-SEM FEI Nova NANOSEM 230 equipment was also used for the study of microstructure of the ceramics used in the electrical characterization of quaternary sulfides.

## 2.4 DTA-TG analysis

The thermal behavior of the activated mixtures was investigated by differential thermal (DTA) and thermogravimetric analysis (TG). The measured were carried out in argon, from room temperature to 1000°C, using a Simultaneous Thermal Analysis, NETZCH STA 409. The heating-cooling rates were 10°C/min and the quantity of sample used was about 20 mg.

## 2.5 Raman spectroscopy

The Raman spectra in selected crystals and powder samples were recorded in the frequency range between 150 and 3500  $\text{cm}^{-1}$  using a micro-Raman Renishaw system 1000 equipped with Leica-DMLM microscope. The spectra data were collected at room temperature with laser line of 633 nm and laser power of 1 mW.

## 2.6 Processing of Ceramics

Synthesized fine powders were used as precursors to process  $\text{Cu}_2\text{Fe}_{1-x}\text{Co}_x\text{SnS}_4$  ( $x = 0.6$  and 1) ceramics. Powders were shaped by isostatically pressing at 312 MPa as thin disks of 6 mm diameter and 0.6 mm thickness. These disks reached densification of about 75%, and finally conventional sintering was carried out in evacuated quartz ampoules with Argon atmosphere, placed in a programmable furnace was reached at temperatures from 700 to 800 °C with a heating rate of 5 °C/min. The density of the ceramics was obtained by the Archimedes method with paraffin.

## 2.7 Electrical properties

Au electrodes were sputtered on the major faces on the thinned ceramic discs for electrical characterization. The dependence of the dielectric permittivity on the temperature at frequencies between 10 kHz and 1 MHz was measured with a HP4194A impedance analyzer, were carried out from 77 to 280 K during heating at 1.5 °C/min.

## RESULTS AND DISCUSSION

Ceramic materials are based on polycrystalline samples obtained through a preparation process that includes the synthesis of the precursor powder

(proposed quaternary sulfides), pressing to form cylindrical pellets and, finally, sintering, during which the densification and growth of ceramic grain occurs.

3.1 Synthesis, X-ray powder diffraction and compositional characterization

The quantitative contents of the constituent elements were examined by an energy dispersive SEM-EDS analysis of the pelletized materials over many grains and micro-crystals. It was found that the average concentrations of the elements Cu, Fe, Co, Sn, and S were close to nominal compositions (Table 1).

**Table 1.** Chemical composition analysis (% mass) of  $\text{Cu}_2\text{Fe}_{1-x}\text{Co}_x\text{SnS}_4$  and end-members.

Cu	Fe	Co	Sn	S	Nominal
30.7	0	12.1	27.9	29.3	$\text{Cu}_2\text{CoSnS}_4$
29.4	3.0	10.8	27.4	29.4	$\text{Cu}_2\text{Fe}_{0.2}\text{Co}_{0.8}\text{SnS}_4$
29.6	5.8	8.6	27.8	28.2	$\text{Cu}_2\text{Fe}_{0.4}\text{Co}_{0.6}\text{SnS}_4$
29.6	7.9	5.2	27.7	29.6	$\text{Cu}_2\text{Fe}_{0.6}\text{Co}_{0.4}\text{SnS}_4$
29.9	10.3	2.6	30.0	28.2	$\text{Cu}_2\text{Fe}_{0.8}\text{Co}_{0.2}\text{SnS}_4$
29.1	12.9	0	28.4	29.6	$\text{Cu}_2\text{FeSnS}_4$

The X-ray powder patterns (XRD) showed sharp lines that reflected the crystallinity and homogeneity of the samples. Representative diffraction profiles are shown in Figure 1. The experimental XRD powder patterns of the solid solutions were compared with simulated XRD patterns (from single-crystal X-ray diffraction data). The XRD patterns of the solid solutions of  $\text{Cu}_2\text{Fe}_{1-x}\text{Co}_x\text{SnS}_4$  ( $x = 0.2, 0.4, 0.6$  and  $0.8$ ) were fully indexed in the space group,  $I-42m$ , and were found to have a stannite-type structure (Figure 2). We propose that these samples existed as a continuous solid solution on the basis of the cell parameter trends determined by X-ray powder diffraction data (Table 2).

**Table 2.** Cell parameters data for  $\text{Cu}_2\text{Fe}_{1-x}\text{Co}_x\text{SnS}_4$  and end-members (space group  $I-42m$ ).

Phase	a(Å)	b(Å)	Vol.(Å <sup>3</sup> )
$\text{Cu}_2\text{CoSnS}_4$	$5.40 \pm 0.03$	$10.79 \pm 0.01$	314.1
$\text{Cu}_2\text{Fe}_{0.2}\text{Co}_{0.8}\text{SnS}_4$	$5.40 \pm 0.04$	$10.83 \pm 0.01$	315.8
$\text{Cu}_2\text{Fe}_{0.4}\text{Co}_{0.6}\text{SnS}_4$	$5.40 \pm 0.03$	$10.81 \pm 0.01$	315.5
$\text{Cu}_2\text{Fe}_{0.6}\text{Co}_{0.4}\text{SnS}_4$	$5.41 \pm 0.05$	$10.80 \pm 0.01$	316.4
$\text{Cu}_2\text{Fe}_{0.8}\text{Co}_{0.2}\text{SnS}_4$	$5.43 \pm 0.03$	$10.78 \pm 0.01$	317.4
$\text{Cu}_2\text{FeSnS}_4$	$5.43 \pm 0.04$	$10.73 \pm 0.01$	316.9

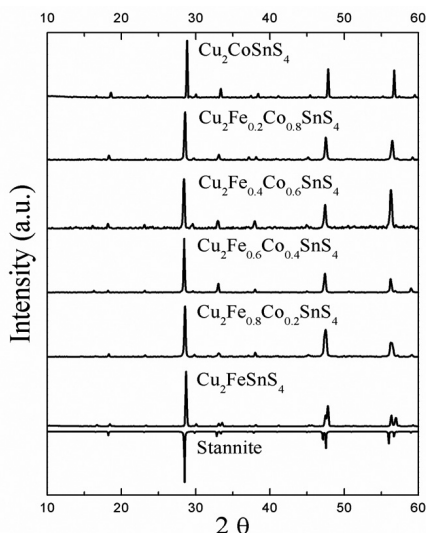


**Figure 1.** X-ray powder diffraction patterns obtained for  $\text{Cu}_2\text{Fe}_{1-x}\text{Co}_x\text{SnS}_4$  ( $x = 0, 0.2, 0.4, 0.6, 0.8$  and  $1.0$ ). The mirror-like representation shows the calculated powder patterns of stannite [8]

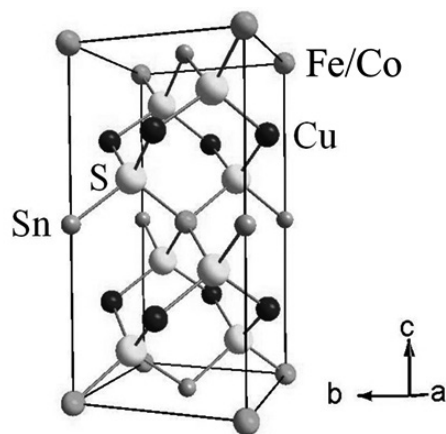


**Figure 2.** Unit Cell of  $\text{Cu}_2\text{Fe}_{1-x}\text{Co}_x\text{SnS}_4$  stannite-type [8]

The TGA and DTA were carried out under an argon atmosphere to study the thermal stability. Figure 3 shows the thermal analysis of  $\text{Cu}_2\text{Fe}_{0.4}\text{Co}_{0.6}\text{SnS}_4$ . The studied phases all exhibited similar behaviors, and all of the phases were stable up to approximately 800 °C. Above this temperature the samples began to decompose. The DTA, in all of the samples, presented an important endothermic signal, which is consistent with an incongruent melting point that has also reported for the related compounds  $\text{Cu}_2\text{MnSnSe}_4$  [16],  $\text{Cu}_2\text{ZnSnSe}_4$ ,  $\text{Cu}_2\text{ZnGeSe}_4$ ,  $\text{Cu}_2\text{CdSnSe}_4$  [17] and  $\text{Cu}_2\text{MnGe}_x\text{Sn}_{1-x}\text{S}_4$  [18] (Table 3).

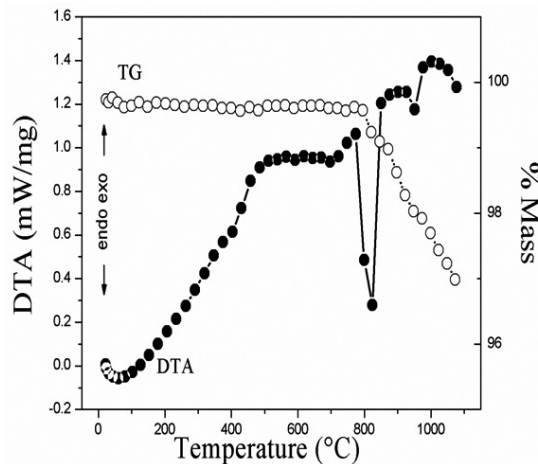


**Figure 3.** Thermal analysis (DTA/TG) of  $\text{Cu}_2\text{Fe}_{0.4}\text{Co}_{0.6}\text{SnS}_4$

**Table 3.** Melting points of quaternary chalcogenides.

Phase	M.P. (°C)		Ref.
$\text{Cu}_2\text{ZnGeSe}_4$	890	Stannite	[17]
$\text{Cu}_2\text{ZnSnSe}_4$	805	Stannite	[17]
$\text{Cu}_2\text{CdSnSe}_4$	780	Stannite	[17]
$\text{Cu}_2\text{MnSnSe}_4$	800	Stannite	[1]

The Raman spectra (Figure 4) showed two main peaks; the most intense peak occurred at approximately 320  $\text{cm}^{-1}$ , and a smaller shoulder was found at 290  $\text{cm}^{-1}$ , which can be assigned to the symmetry mode (A1). These vibrations can be interpreted as the “breathing” mode of the  $\text{MS}_4$  tetrahedral ( $M = \text{Fe, Co}$ ) and  $\text{SnS}_4$ , according to the assignment proposed by Koschel et al. [19,20]. Finally, there was no evidence supporting the presence of metal polysulfide impurities of the types  $\text{Cu}_2\text{FeS}_2$ ,  $\text{Cu}_2\text{CoS}_2$  and  $\text{SnS}_2$  due to the absence of signals at 350  $\text{cm}^{-1}$ , which are characteristic of this type of compounds [21,22].

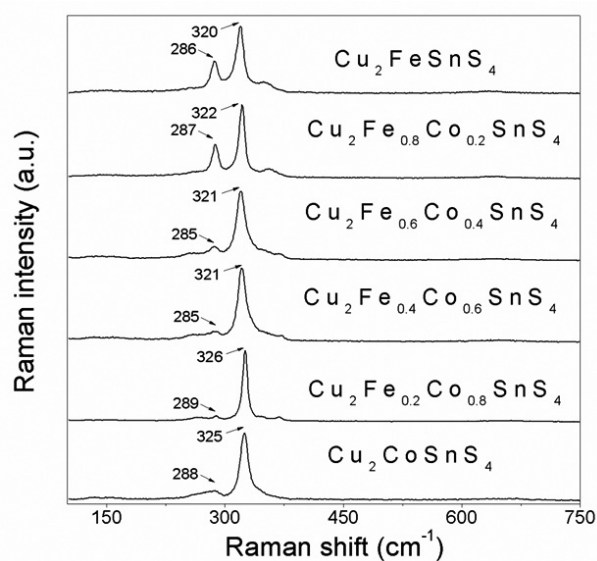


Figure 4. Raman spectra of  $\text{Cu}_2\text{Fe}_x\text{Co}_{1-x}\text{SnS}_4$  solid solutions ( $0 < x < 1$ )

### 3.2 Ceramic Processing

Different sintering tests were carried out on the studied phases of  $\text{Cu}_2\text{Fe}_x\text{Co}_{1-x}\text{SnS}_4$ . The end-member  $\text{Cu}_2\text{FeSnS}_4$  could not be prepared as a ceramic, possibly, because in the thermal process, the grain size increased so rapidly that pores were generated between the grains, which decreased the hardness of  $\text{Cu}_2\text{FeSnS}_4$  to the point of becoming brittle. However, the other end-member,  $\text{Cu}_2\text{CoSnS}_4$ , was transformed into a ceramic with a 97% densification. In general, the Corich phases were able to transform into ceramics with densifications greater than 80%. It should be noted that the chosen temperatures were based on the DTA-TG because in the preparation of ceramics, the melting point must not be exceeded. The percentage of densification as a function of the temperature of the phase of  $\text{Cu}_2\text{Fe}_{0.4}\text{Co}_{0.6}\text{SnS}_4$  is shown in Figure 5. The curve, characteristic of this type of phenomenon, demonstrates a temperature zone (25-600 °C) in which there was practically no variation in density. Then, a second zone was observed with an increase in the densification percentage where temperature variations of 50 °C caused important changes in the densities.

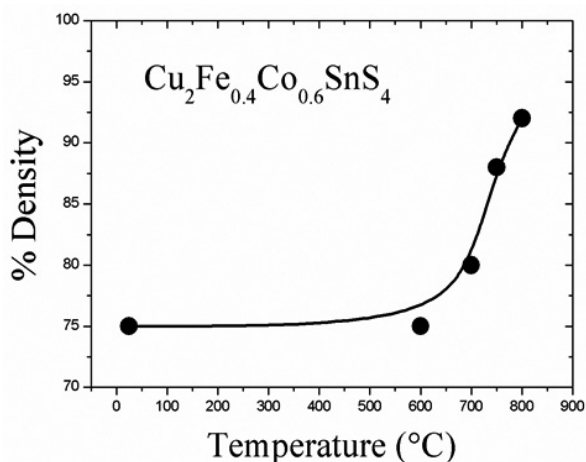


Figure 5.  $\text{Cu}_2\text{Fe}_{0.4}\text{Co}_{0.6}\text{SnS}_4$  density as a function of temperature with an increase of grain size.

The DRX on the sides of the pellets prepared with  $\text{Cu}_2\text{Fe}_{0.4}\text{Co}_{0.6}\text{SnS}_4$  confirmed the presence of the studied phase and discarded the presence of secondary phases (Figure 6). With a gradual increase in the density, it was possible to observe that there was a widening of signals, which was the product of the overlapping growth of the grain. Therefore, the structural changes in the material do not occur in the formation of the ceramics.

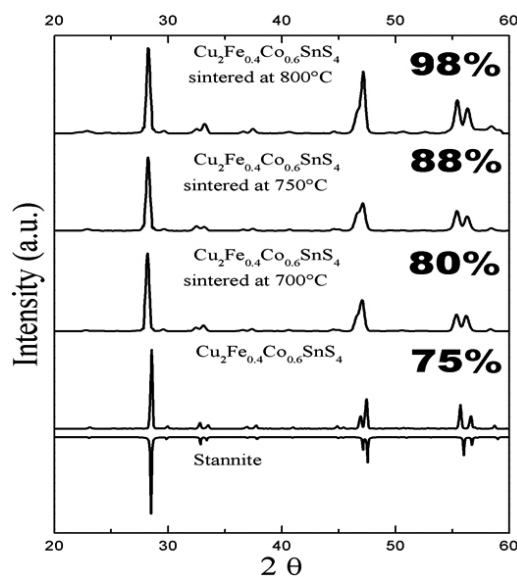


Figure 6. X-ray diffraction of  $\text{Cu}_2\text{Fe}_{0.4}\text{Co}_{0.6}\text{SnS}_4$  pellets with densities of 75%, 80%, 88%, and 98%. (bottom) The mirror-like representation shows the calculated powder patterns of stannite [8]

Figure 7 shows the FE-SEM backscattered electron images of the polished surfaces of the sintered  $\text{Cu}_2\text{Fe}_{0.4}\text{Co}_{0.6}\text{SnS}_4$  ceramics at different temperatures: at 700 °C the grain size ranged from 3-5 μm, at 750 °C from 20-30 μm and finally at 800 °C increases the grain size between 60-100 μm. These images corroborate the aforementioned increase in size of the grains with increasing temperature.

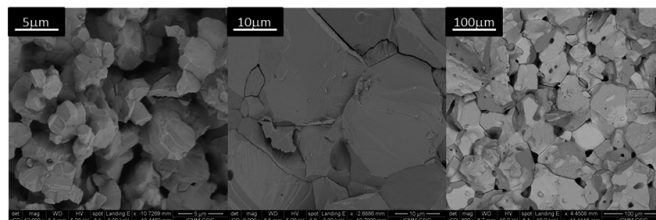


Figure 7. Micrographs of the polished surfaces of  $\text{Cu}_2\text{Fe}_{0.4}\text{Co}_{0.6}\text{SnS}_4$  ceramics sintered at 700 °C, 750 °C and 800 °C.

### 3.3 Electrical Characterization

The end-members of the  $\text{Cu}_2\text{Fe}_x\text{Co}_{1-x}\text{SnS}_4$  solid solution presented totally different electrical behaviors. The  $\text{Cu}_2\text{FeSnS}_4$  phase was measured in a pellet without sintering using the Van der Pauw method. This phase presented the behavior of a semiconductor with a conductivity of 0.071 S/cm at 250 K, which is a greater conductivity value than in single crystals of  $\text{Cu}_2\text{CdGeS}_4$  (0.003 S/cm at 250 K) [12]. For its part,  $\text{Cu}_2\text{CoSnS}_4$ , which was transformed into a ceramic with a 97% densification, was measured with the impedance complex, which showed that it had the electrical behaviour of a semiconductor with a conductivity of 30 S/cm at 250 K. This conductivity is greater than that of the crystalline powder of  $\text{Cu}_2\text{MnSnS}_4$  (0.10 S/cm at 296 K) [1]. In the plot of the electrical conductivity as a function of the inverse of the temperature (Figure 8), three changes in the slope were observed, which can be interpreted as; a zone in which the conductivity is dominated by free charge carriers (high temperature) and in another dominating hopping type mechanism [12].

An interesting electrical behaviour was observed in the phase  $\text{Cu}_2\text{Fe}_{0.4}\text{Co}_{0.6}\text{SnS}_4$ . The electrical characterization of this ceramic, processed at 800 °C with a 98% densification, was performed using complex impedance. In this solid solution, the electric conductivity presented Arrhenius behaviour over the measured temperature range (80-300 K), indicating a thermally activated process with an activation energy of 0.067 eV (Figure 9). This activation energy was in accordance with the values reported for the single crystals of the related phases  $\text{Cu}_2\text{CdGeS}_4$  (0.025 eV) [12],  $\text{Cu}_2\text{MnSnS}_4$  (0.030 eV) [1] and  $\text{Cu}_2\text{CoGeS}_4$  (0.030 eV) [1].

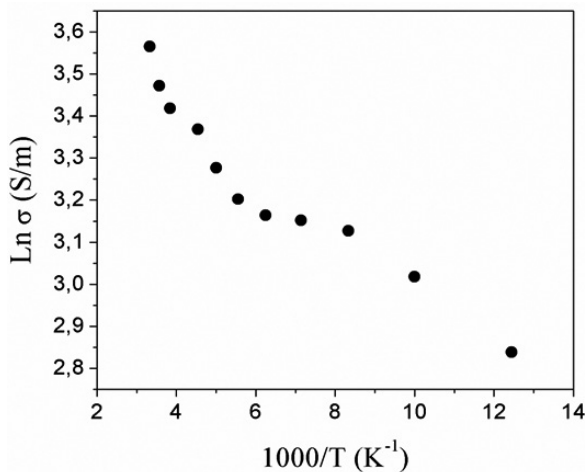


Figure 8. Conductivity versus temperature for  $\text{Cu}_2\text{CoSnS}_4$  with density 85%.

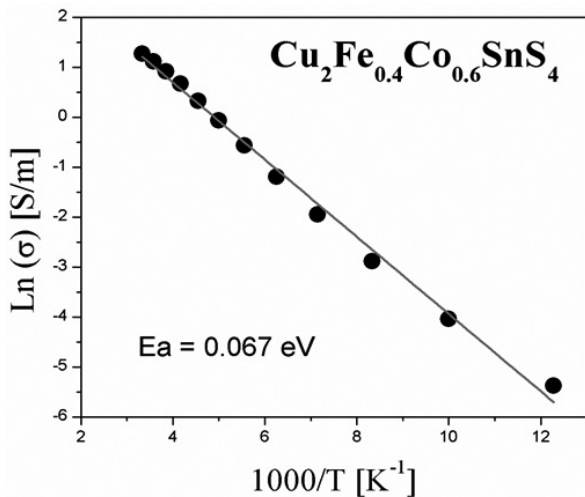


Figure 9. Arrhenius plot of  $\text{Cu}_2\text{Fe}_{0.4}\text{Co}_{0.6}\text{SnS}_4$ .

Figure 10 shows a plot of the real permittivity as a function of temperature. It can be observed that the electrical response due to the typical relaxation behavior in this frequency range at temperatures ranging from 100 to 250 K, with a maximum temperature of 200 K, was frequency independent. However, the imaginary component presented a constant increase over the entire range of frequencies. It is possible to suggest a space charge polarization mechanism is responsible for this electrical relaxation. It is known that quasi-free carriers can originate a space charge at the electrode/sample interfaces [23], and the application of an electric field breaks the symmetry of the space charge and creates macroscopic dipoles, these dipoles lead to dielectric relaxation. The space charge polarization model is often used to explain the experimental results in grain boundary layer capacitors, where the grains are semiconductors and the grain boundaries are insulators [24].

### CONCLUSIONS

The solid solutions  $\text{Cu}_2\text{Fe}_{1-x}\text{Co}_x\text{SnS}_4$  ( $x = 0.2; 0.4; 0.6$  and  $0.8$ ) were fully indexed in the space group I-42m, in a stannite-type. These phases are stable up to approximately 800° C and present incongruent melting. In general, Corrich phases formed ceramics with percentages of densification above 80%. The phases of the  $\text{Cu}_2\text{Fe}_{1-x}\text{Co}_x\text{SnS}_4$  showed electrical behavior of semiconductors. In particular, the  $\text{Cu}_2\text{Fe}_{0.4}\text{Co}_{0.6}\text{SnS}_4$  presents dielectric relaxation between 100 and 250 K, with a maximum at approximately 200 K, the electric permittivity found has orders of magnitude between  $10^2$  and  $10^3$ , so it can be estimated that this phase presents important contributions of electron polarization.

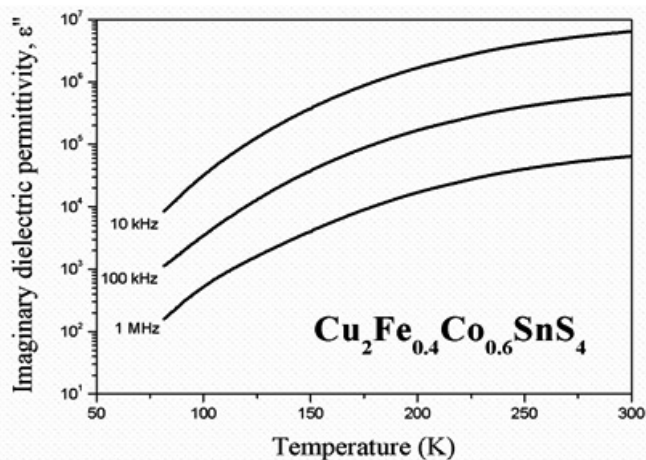
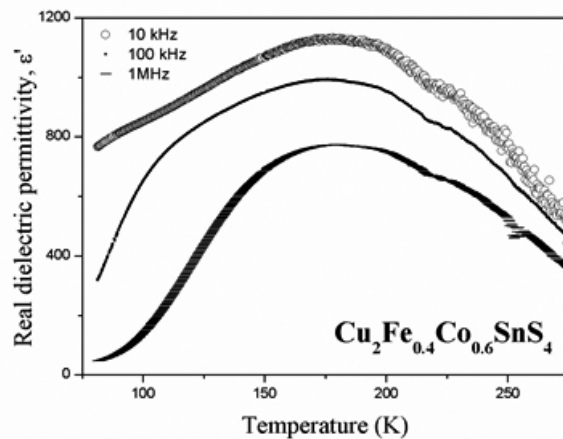


Figure 10.  $\text{Cu}_2\text{Fe}_{0.4}\text{Co}_{0.6}\text{SnS}_4$ : a) Real permittivity versus temperature at different frequencies, b) Imaginary permittivity versus temperature at different frequencies.

### ACKNOWLEDGEMENTS

The authors wish to dedicate this work to the memory of Dr. Juan Guillermo Contreras, a fine Professor and a very good friend. This work was supported by Becas Chile de Pasantía Doctoral en el Extranjero 2011-75110054. The collaboration of Dr. Miguel Algueró (ICMM-CSIC) in the electrical characterization is greatly acknowledged.

### REFERENCES

1. L. Guen, W.S. Glaunsinger, *Journal of Solid State Chemistry* **21** (1980) 10–21.
2. C. Persson, *Journal of Applied Physics* **107** (2010) 053710.
3. D.A.R. Barkhouse, O. Gunawan, T. Gokmen, T.K. Todorov, D.B. Mitzi, *Progress in Photovoltaics: Research and Applications* **20** (2012) 6–11.
4. J.P. Leitão, N.M. Santos, P. a. Fernandes, P.M.P. Salomé, a. F. da Cunha, J.C. González, G.M. Ribeiro, F.M. Matinaga, *Physical Review B* **84** (2011) 024120.
5. X. Wu, W. Liu, S. Cheng, Y. Lai, H. Jia, *Journal of Semiconductors* **33** (2012) 022002.
6. H. Yang, L. a Jauregui, G. Zhang, Y.P. Chen, Y. Wu, *Nano Letters* **12** (2012) 540–545.
7. X.Y. Shi, F.Q. Huang, M.L. Liu, L.D. Chen, *Applied Physics Letters* **94** (2009) 122103.
8. S.R. Hall, J.T. Szymanski, J.M. Stewart, *Canadian Mineralogist* **16** (1978) 131–137.
9. S. Schorr, H.A.-J.O. Hoebler, M.I. Tovar, *European Journal of Mineralogy* **19** (2007) 65–73.
10. E. Quintero, M. Quintero, E. Moreno, L. Lara, M. Morocoima, F. Pineda, P. Grima, R. Tovar, P. Bocaranda, J. a. Henao, M. a. Macias, *Journal of*

- Physics and Chemistry of Solids* **71** (2010) 993–998.
11. T. Fries, Y. Shapira, F. Palacio, M.C. Moro, G.J. McIntyre, R. Kershaw, A. Wold, E.J. McNiff Jr., *Physical Review B* **56** (1997) 5424–5431.
  12. G.E. Davidyuk, O. V Parasyuk, S.A. Semenyuk, Y.E. Romanyuk, *Inorganic Materials* **39** (2003) 919–923.
  13. K. Timmo, M. Altosaar, J. Raudoja, K. Muska, M. Pilvet, M. Kauk, T. Varema, M. Danilson, O. Volobujeva, E. Mellikov, *Solar Energy Materials and Solar Cells* **94** (2010) 1889–1892.
  14. F. López-Vergara, A. Galdámez, V. Manríquez, P. Barahona, O. Peña, *Journal of Solid State Chemistry* **198** (2013) 386–391.
  15. P. for the I. of X. experiments CHECKCELL, J. Laugier, B. Bochu, Laboratoire Des Matériaux et Du Génie Physique Ecole Nationale Supérieure de Physique de Grenoble (INPG) Domaine Universitaire BP 46, 38402 Saint Martin d'Hères France, <http://www.inpg.fr/LMGP> (n.d.).
  16. V.W. Schäfer, R. Nitsche, *Zeitschrift Für Kristallographie* **145** (1977) 356–370.
  17. H. Matsushita, T. Maeda, A. Katsui, T. Takizawa, *Journal of Crystal Growth* **208** (2000) 416–422.
  18. T. Bernert, M. Zabel, A. Pfitzner, *Journal of Solid State Chemistry* **179** (2006) 849–854.
  19. M. Altosaar, J. Raudoja, K. Timmo, M. Danilson, M. Grossberg, J. Krustok, E. Mellikov, *Physica Status Solidi (a)* **205** (2008) 167–170.
  20. W.H. Koschel, F. Sorger, J. Baars, *Journal of Physiques Colloques* **36** (1975) 177–181.
  21. P.A. Fernandes, P.M.P. Salomé, A.F. Cunha, *Thin Solid Films* **517** (2009) 2519–2523.
  22. M. Himmrich, H. Haeuseler, *Spectrochimica Acta Part A: Molecular Spectroscopy* **47** (1991) 933–942.
  23. A.K. Jonscher, *Journal of Physics D: Applied Physics* **57** (1999) R57–R70.
  24. I. Burn, S. Neirman, *Journal of Materials Science* **17** (1982) 3510–3524.